REPORT DOCUMENTATION PAGE

Form Approved OMB NO. 0704-0188

1. REPORT DATE (DD-MM-YYYY)	2. REPORT TYPE	3. DATES COVERED (From - To)
31-03-2014	Final Report	1-Oct-2010 - 31-Dec-2013

4. TITLE AND SUBTITLE
Ultra-high Strength Nanostructured Mg

5a. CONTRACT NUMBER
W911NF-10-1-0512

5b. GRANT NUMBER

5c. PROGRAM ELEMENT NUMBER
611102

6. AUTHORS
Enrique J. Lavernia

5d. PROJECT NUMBER

5e. TASK NUMBER

5f. WORK UNIT NUMBER

7. PERFORMING ORGANIZATION NAMES AND ADDRESSES
University of California - Davis
Office Of Research
1850 Research Park Dr. Suite 300
Davis, CA 95618 -6153

8. PERFORMING ORGANIZATION REPORT NUMBER

9. SPONSORING/MONITORING AGENCY NAME(S) AND ADDRESS (ES)
U.S. Army Research Office
P.O. Box 12211
Research Triangle Park, NC 27709-2211

10. SPONSOR/MONITOR'S ACRONYM(S)
ARO

11. SPONSOR/MONITOR'S REPORT NUMBER(S)
58330-MS.10

12. DISTRIBUTION AVAILIBILITY STATEMENT
Approved for Public Release; Distribution Unlimited

13. SUPPLEMENTARY NOTES
The views, opinions and/or findings contained in this report are those of the author(s) and should not contrued as an official Department of the Army position, policy or decision, unless so designated by other documentation.

14. ABSTRACT
The technological goal of the research program was to develop Mg alloys with revolutionary mechanical properties by taking advantage of our fundamental knowledge of the interactions between multiscale microstructures (i.e., nano-grain, micron-grain, and amorphous). The scientific goal of the research was to provide fundamental insight into novel phenomena, plasticity mechanisms in HCP systems, the relationship between twin characteristics and grain size, and strengthening and plasticity mechanisms in Mg. Key research activities conducted during the performance period of 10/1/2010-12/31/2013 include: (1) synthesis of nanostructured pure Mg and Mg alloy

15. SUBJECT TERMS
Nanostructured Mg and Mg alloys, Mg metallic glass, Cryomilling, Powder consolidation, Spark plasma sintering, Deformation mechanisms

16. SECURITY CLASSIFICATION OF:			17. LIMITATION OF ABSTRACT	15. NUMBER OF PAGES	19a. NAME OF RESPONSIBLE PERSON
a. REPORT	b. ABSTRACT	c. THIS PAGE			Enrique Lavernia
UU	UU	UU	UU		19b. TELEPHONE NUMBER 530-752-0554

Report Title

Ultra-high Strength Nanostructured Mg

ABSTRACT

The technological goal of the research program was to develop Mg alloys with revolutionary mechanical properties by taking advantage of our fundamental knowledge of the interactions between multiscale microstructures (i.e., nano-grain, micron-grain, and amorphous). The scientific goal of the research was to provide fundamental insight into novel phenomena, plasticity mechanisms in HCP systems, the relationship between twin characteristics and grain size, and strengthening and plasticity mechanisms in Mg. Key research activities conducted during the performance period of 10/1/2010-12/31/2013 include: (1) synthesis of nanostructured pure Mg and Mg alloy powders by cryomilling; (2) analysis of deformation twinning in nanostructured Mg and Mg alloy powders; (3) synthesis, microstructural and mechanical characterization of bulk nanostructured pure Mg and Mg alloys; (4) synthesis of nanostructured Mg-Y powders by gas atomization and cryomilling; (5) investigation of stacking faults and twinning in ultrafine grained Mg-Y alloy; (6) mechanical characterization of ultrafine grained Mg-Y alloy; (7) dynamic grain refinement in nanostructured Mg and Mg-Y deformed at cryogenic temperatures; (8) influence of mechanically milled powder and high pressure on spark plasma sintering of Mg-Cu-Gd metallic glasses; (9) microstructure and mechanical behavior of Mg-10Li-3Al-2.5Sr alloy; (10) influence of extrusion on microstructure and mechanical behavior of Mg-9Li-3Al-xSr alloys; (11) study of multiple and extended shear band formation in MgCuGd metallic glass during high pressure torsion; and (12) observation of prism stacking faults contiguous to a {10-12} twin in a Mg–Y alloy.

Enter List of papers submitted or published that acknowledge ARO support from the start of the project to the date of this printing. List the papers, including journal references, in the following categories:

(a) Papers published in peer-reviewed journals (N/A for none)

Received		Paper
08/30/2011	1.00	Baolong Zheng, Osman Ertorer, Ying Li, Yizhang Zhou, Suveen N. Mathaudhub, Chi Y.A. Tsao, Enrique J. Lavernia. High strength, nano-structured Mg–Al–Zn alloy, Materials Science and Engineering, (02 2011): 2180. doi:
09/30/2013	5.00	Baolong Zheng, Dustin Ashford, Yizhang Zhou, Suveen N. Mathaudhu, Jean-Pierre Delplanque, Enrique J. Lavernia. Influence of mechanically milled powder and high pressure on spark plasma sintering of Mg–Cu–Gd metallic glasses, Acta Materialia , (07 2013): 4414. doi:
09/30/2013	6.00	Baolong Zheng, Ying Li, Weizong Xu, Yizhang Zhou, Suveen N. Mathaudhu, Yuntian Zhu and Enrique J. Lavernia. Twinning in cryomilled nanocrystallineMg powder, Philosophical Magazine Letters, (06 2013): 457. doi:
09/30/2013	7.00	YAN YANG, XIAODONG PENG, HAIMING WEN, BAOLONG ZHENG, YIZHANG ZHOU, WEIDONG XIE, and ENRIQUE J. LAVERNIA. Influence of Extrusion on the Microstructure and MechanicalBehavior of Mg-9Li-3Al-xSr Alloys, METALLURGICAL AND MATERIALS TRANSACTIONS A, (02 2013): 1101. doi:
TOTAL:	**4**	

Number of Papers published in peer-reviewed journals:

(b) Papers published in non-peer-reviewed journals (N/A for none)

Received		Paper
03/26/2014	8.00	Dalong Zhang, Baolong Zheng, Yizhang Zhou, Subhash Mahajan, Enrique J. Lavernia. Prism stacking faults observed contiguous to a {10-12} twin in a Mg–Y alloy, Scripta Materialia, (12 2013): 61. doi:
TOTAL:	**1**	

Number of Papers published in non peer-reviewed journals:

(c) Presentations

1) Baolong Zheng, Osman Ertorer, Ying Li, Troy Topping, Yizhang Zhou, Chi Y.A. Tsao, and Enrique J. Lavernia, Nano-Structured Mg-Al-Zn alloy via Cryomilling and Spark Plasma Sintering, TMS2011, San Diego, CA. 2/27-3/3/2011 (2nd Place Awards).
2) Baolong Zheng, Yizhang Zhou, Chi Y.A. Tsao, Ruslan Z. Valiev, and Enrique J. Lavernia, On Interfacial Bonding in Mg-Cu-Gd Metallic Glass via High Pressure Torsion (HPT), TMS2011, San Diego, CA. February 27 – March 3, 2011.
3) B. Zheng, T. Topping, Y. Zhou, S.N. Mathaudhu, and E.J. Lavernia, Microstructure and Mechanical Properties of Nanocrystalline Pure Mg via Cryomilling, Spark Plasma Sintering and Extrusion, TMS2012, Orlando, FL, 03/11-15/2012. (Best Poster Award).
4) B. Zheng, Y. Li, Weizong Xu, Y. Zhou, S.N. Mathaudhu, Y. Zhu, and E.J. Lavernia, Twinning phenomena in cryomilled pure Mg and Mg-Al-Zn alloy nanocrystalline powders, TMS2012, Orlando, FL, 03/11-15/2012.
5) S.N. Mathaudhu, B. Zheng, K. Youssef, M. Pozuelo, L. Kecskes, Y. Zhou, W. Kao, S. Kim, B. Li, X. Wu, C. Koch, J.M. Yang, E.J. Lavernia, and Y. Zhu, Deformation Twinning in nanocrystalline Mg alloy, TMS2012, Orlando, FL, 03/11-15/2012. (Invited)
6) Suveen N. Mathaudhu, Enrique J. Lavernia, Baolong Zheng, Dustin Ashford, Yizhang Zhou, and Jean-Pierre Delplanque, Microstructure and Behavior of Nano-Structured Mg and Mg Alloys via Cryomilling and Spark Plasma Sintering, PowderMet 2012, Nashville, TN, 06/10-13/2012. (Invited)
7) Suveen N. Mathaudhu, Weizong Xu, Baolong Zheng, Yuntian. T. Zhu, and Enrique Lavernia, A Rationale for Deformation Twinning in Nanocrystalline Magnesium and Magnesium AZ80 Alloy, 9th International Conference on Magnesium Alloys and their Applications, Vancouver, Canada, 07/08-12, 2012. (Invited)
8) Dalong Zhang, Baolong Zheng, Yizhang Zhou, Suveen Mathaudhu, Yuntian Zhu, Enrique Lavernia, " Fabrication and Characterization of Nanocrystalline Mg-Y alloy", Materials Science & Technology 2012, October, Pittsburgh, PA.
9) Dalong Zhang, Baolong Zheng, Yizhang Zhou, Suveen Mathaudhu, Enrique Lavernia, "Deformation Behavior of Nanocrystalline Mg-Y Alloy", the 2013 TMS Annual Meeting & Exhibition, March 3–7 San Antonio, Texas.
10) Baolong Zheng, Dalong Zhang, Yizhang Zhou, Suveen N. Mathaudhu, Deepak Kapoor, Joseph Paras, and Enrique J. Lavernia, Dynamic Grain Refinement in Nanostructured Mg and Mg-Y Deformed at Cryogenic Temperatures, PowderMet 2013, Chicago, IL, June 24-27, 2013;
11) Baolong Zheng, Yizhang Zhou, Suveen N. Mathaudhu, and Enrique J. Lavernia, Dynamic grain refinement for nanostructured pure Mg powder processed via cryogenic temperature deformation of cryomilling, the 2013 TMS Annual Meeting & Exhibition, March 3–7 San Antonio, Texas.
12) Yan Yang, Xiaodong Peng, Baolong Zheng, Yizhang Zhou, Enrique J. Lavernia, Microstructure and Mechanical Properties of Nanocrystalline Mg-9Li-3Al-2.5Sr Alloy via Cryomilling and Spark Plasma Sintering, the 2013 TMS Annual Meeting & Exhibition, March 3–7 San Antonio, Texas.
13) Dalong Zhang, Baolong Zheng, Yizhang Zhou, Suveen Mathaudhu, Enrique Lavernia, "Deformation Behavior of Nanocrystalline Mg-Y Alloy", the 2013 TMS Annual Meeting & Exhibition, March 3–7 San Antonio, Texas.
14) A Williamson, B Zheng, E Lavernia, J Groza, J-P Delplanque, Investigation of Pressure and Thermal Behavior during Spark Plasma Sintering on Grain Growth, TMS2014, San Diego, CA. February 16-20, 2014.

Number of Presentations: 14.00

Non Peer-Reviewed Conference Proceeding publications (other than abstracts):

Received	Paper

TOTAL:

Number of Non Peer-Reviewed Conference Proceeding publications (other than abstracts):

Peer-Reviewed Conference Proceeding publications (other than abstracts):

Received	Paper

TOTAL:

Number of Peer-Reviewed Conference Proceeding publications (other than abstracts):

(d) Manuscripts

Received		Paper
03/31/2014	9.00	Baolong Zheng, Yizhang Zhou, Suveen N. Mathaudhu, Ruslan Z. Valiev, Chi Y.A. Tsao, Julie, M. Schoenung, Enrique J. Lavernia . Multiple and Extended Shear Band Formation in MgCuGd Metallic Glass during High Pressure Torsion, Scripta Materialia (01 2014)
08/30/2012	2.00	. Influence of Mechanically Milled Powder and High Pressure on Spark Plasma Sintering of Mg-Cu-Gd Metallic Glasses, ( )
08/31/2012	3.00	. Influence of extrusion on the microstructure and mechanical behavior of Mg-9Li-3Al-xSr alloys, METALLURGICAL AND MATERIALS TRANSACTIONS A (02 2012)
TOTAL:		**3**

Number of Manuscripts:

Books

Received Paper

TOTAL:

Patents Submitted

Patents Awarded

Awards

2014 Fellow, TMS
Member, National Academy of Engineering, 2013
Fellow, Materials Research Society (MRS), 2013
ASM 2013 Edward DeMille Campbell Memorial Lectureship
ASM International; ASM International 2013 Gold Medal Award, ASM International
Hispanic Engineer National Achievement Award (HEENAC), Great Minds in STEM, 2011
2011 SACNAS Distinguished Scientist, Society for Advancement of Chicanos and Native Americans in Science (SACNAS)

Graduate Students

NAME	PERCENT_SUPPORTED	Discipline
Dalong Zhang	1.00	
Yan Yang	0.00	
FTE Equivalent:	**1.00**	
Total Number:	**2**	

Names of Post Doctorates

NAME	PERCENT_SUPPORTED
Osman Ertorer	0.10
Baolong Zheng	0.36
FTE Equivalent:	**0.46**
Total Number:	**2**

Names of Faculty Supported

NAME	PERCENT_SUPPORTED	National Academy Member
Enrique Lavernia	0.00	Yes
FTE Equivalent:	**0.00**	
Total Number:	**1**	

Names of Under Graduate students supported

NAME	PERCENT_SUPPORTED	Discipline
Joshua Pegadiotes	0.00	Mechanical Engineering
FTE Equivalent:	**0.00**	
Total Number:	**1**	

Student Metrics

This section only applies to graduating undergraduates supported by this agreement in this reporting period

The number of undergraduates funded by this agreement who graduated during this period:	1.00
The number of undergraduates funded by this agreement who graduated during this period with a degree in science, mathematics, engineering, or technology fields:	1.00
The number of undergraduates funded by your agreement who graduated during this period and will continue to pursue a graduate or Ph.D. degree in science, mathematics, engineering, or technology fields:	0.00
Number of graduating undergraduates who achieved a 3.5 GPA to 4.0 (4.0 max scale):	0.00
Number of graduating undergraduates funded by a DoD funded Center of Excellence grant for Education, Research and Engineering:	0.00
The number of undergraduates funded by your agreement who graduated during this period and intend to work for the Department of Defense	0.00
The number of undergraduates funded by your agreement who graduated during this period and will receive scholarships or fellowships for further studies in science, mathematics, engineering or technology fields:	0.00

Names of Personnel receiving masters degrees

NAME
Total Number:

Names of personnel receiving PHDs

NAME
Total Number:

Names of other research staff

NAME	PERCENT_SUPPORTED
Yizhang Zhou	0.00
FTE Equivalent:	**0.00**
Total Number:	**1**

Sub Contractors (DD882)

Inventions (DD882)

Scientific Progress

See Attachment

Technology Transfer

REPORT DOCUMENTATION PAGE

Form Approved
OMB NO. 0704-0188

1. AGENCY USE ONLY (Leave Blank)	2. REPORT DATE	3. REPORT TYPE AND DATES COVERED
	03/31/2014	Final Technical Report October 1, 2010 – December 31, 2013

4. TITLE AND SUBTITLE	5. FUNDING NUMBERS
Ultra-high Strength Nanostructured Mg	ARO W911NF10-1-0512
6. AUTHOR(S) Enrique J. Lavernia	

7. PERFORMING ORGANIZATION NAME(S) AND ADDRESS(ES)	8. PERFORMING ORGANIZATION REPORT NUMBER
University of California, Davis One shields Ave Davis, CA 95616	

9. SPONSORING / MONITORING AGENCY NAME(S) AND ADDRESS(ES)	10. SPONSORING / MONITORING AGENCY REPORT NUMBER
U. S. Army Research Office P.O. Box 12211 Research Triangle Park, NC 27709-2211	

11. SUPPLEMENTARY NOTES

The views, opinions and/or findings contained in this report are those of the author(s) and should not be construed as an official Department of the Army position, policy or decision, unless so designated by other documentation.

12 a. DISTRIBUTION / AVAILABILITY STATEMENT	12 b. DISTRIBUTION CODE
Approved for public release; distribution unlimited.	

13. ABSTRACT (Maximum 200 words)

The technological goal of the research program was to develop Mg alloys with revolutionary mechanical properties by taking advantage of our fundamental knowledge of the interactions between multiscale microstructures (i.e., nano-grain, micron-grain, and amorphous). The scientific goal of the research was to provide fundamental insight into novel phenomena, plasticity mechanisms in HCP systems, the relationship between twin characteristics and grain size, and strengthening and plasticity mechanisms in Mg. Key research activities conducted during the performance period of 10/1/2010-12/31/2013 include: (1) synthesis of nanostructured pure Mg and Mg alloy powders by cryomilling; (2) analysis of deformation twinning in nanostructured Mg and Mg alloy powders; (3) synthesis, microstructural and mechanical characterization of bulk nanostructured pure Mg and Mg alloys; (4) synthesis of nanostructured Mg-Y powders by gas atomization and cryomilling; (5) investigation of stacking faults and twinning in ultrafine grained Mg-Y alloy; (6) mechanical characterization of ultrafine grained Mg-Y alloy; (7) dynamic grain refinement in nanostructured Mg and Mg-Y deformed at cryogenic temperatures; (8) influence of mechanically milled powder and high pressure on spark plasma sintering of Mg-Cu-Gd metallic glasses; (9) microstructure and mechanical behavior of Mg-10Li-3Al-2.5Sr alloy; (10) influence of extrusion on microstructure and mechanical behavior of Mg-9Li-3Al-xSr alloys; (11) study of multiple and extended shear band formation in MgCuGd metallic glass during high pressure torsion; and (12) observation of prism stacking faults contiguous to a {10-12} twin in a Mg–Y alloy.

14. SUBJECT TERMS	15. NUMBER OF PAGES
Nanostructured Mg and Mg alloys, Mg metallic glass, Cryomilling, Powder consolidation, Spark plasma sintering, Deformation mechanisms	16. PRICE CODE

17. SECURITY CLASSIFICATION OR REPORT	18. SECURITY CLASSIFICATION ON THIS PAGE	19. SECURITY CLASSIFICATION OF ABSTRACT	20. LIMITATION OF ABSTRACT
UNCLASSIFIED	**UNCLASSIFIED**	**UNCLASSIFIED**	**UL**

REPORT DOCUMENTATION PAGE (SF298)
(Continuation Sheet)

1. List of Publications and Presentations

1) Baolong Zheng, Osman Ertorer, Ying Li, Yizhang Zhou, Suveen N. Mathaudhu, Chi Y.A. Tsao, and Enrique J. Lavernia, "High Strength, Nano-structured Mg–Al–Zn Alloy", Mater. Sci. & Eng. A, Vol. 528, pp. 180-2191, 2011.

2) Baolong Zheng, Osman Ertorer, Ying Li, Troy Topping, Yizhang Zhou, Chi Y.A. Tsao, and Enrique J. Lavernia, Nano-Structured Mg-Al-Zn alloy via Cryomilling and Spark Plasma Sintering, TMS2011, San Diego, CA. 2/27-3/3/2011 (2^{nd} Place Awards).

3) Baolong Zheng, Yizhang Zhou, Chi Y.A. Tsao, Ruslan Z. Valiev, and Enrique J. Lavernia, On Interfacial Bonding in Mg-Cu-Gd Metallic Glass via High Pressure Torsion (HPT), TMS2011, San Diego, CA. February 27 – March 3, 2011.

4) B. Zheng, T. Topping, Y. Zhou, S.N. Mathaudhu, and E.J. Lavernia, Microstructure and Mechanical Properties of Nanocrystalline Pure Mg via Cryomilling, Spark Plasma Sintering and Extrusion, TMS2012, Orlando, FL, 03/11-15/2012. (**Best Poster Award**).

5) B. Zheng, Y. Li, Weizong Xu, Y. Zhou, S.N. Mathaudhu, Y. Zhu, and E.J. Lavernia, Twinning phenomena in cryomilled pure Mg and Mg-Al-Zn alloy nanocrystalline powders, TMS2012, Orlando, FL, 03/11-15/2012.

6) S.N. Mathaudhu, B. Zheng, K. Youssef, M. Pozuelo, L. Kecskes, Y. Zhou, W. Kao, S. Kim, B. Li, X. Wu, C. Koch, J.M. Yang, E.J. Lavernia, and Y. Zhu, Deformation Twinning in nanocrystalline Mg alloy, *TMS2012*, Orlando, FL, 03/11-15/2012. **(Invited)**

7) Suveen N. Mathaudhu, Enrique J. Lavernia, Baolong Zheng, Dustin Ashford, Yizhang Zhou, and Jean-Pierre Delplanque, Microstructure and Behavior of Nano-Structured Mg and Mg Alloys via Cryomilling and Spark Plasma Sintering, PowderMet 2012, Nashville, TN, 06/10-13/2012. **(Invited)**

8) Suveen N. Mathaudhu, Weizong Xu, Baolong Zheng, Yuntian. T. Zhu, and Enrique Lavernia, A Rationale for Deformation Twinning in Nanocrystalline Magnesium and Magnesium AZ80 Alloy, 9th International Conference on Magnesium Alloys and their Applications, Vancouver, Canada, 07/08-12, 2012. **(Invited)**

9) Dalong Zhang, Baolong Zheng, Yizhang Zhou, Suveen Mathaudhu, Yuntian Zhu, Enrique Lavernia, " Fabrication and Characterization of Nanocrystalline Mg-Y alloy", Materials Science & Technology 2012, October, Pittsburgh, PA.

10) Dalong Zhang, Baolong Zheng, Yizhang Zhou, Suveen Mathaudhu, Enrique Lavernia, "Deformation Behavior of Nanocrystalline Mg-Y Alloy", the 2013 TMS Annual Meeting & Exhibition, March 3–7 San Antonio, Texas.

11) Baolong Zheng, Dustin Ashford, Yizhang Zhou, Suveen N. Mathaudhu, Jean-Pierre Delplanque, and Enrique J. Lavernia, Influence of Mechanically Milled Powder and High Pressure on Spark Plasma Sintering of Mg-Cu-Gd Metallic Glasses, Acta Materialia, Vol. 61, pp. 4414-4428, July 2013.

12) Yan Yang, Xiaodong Peng, Haiming Wen, Baolong Zheng, Yizhang Zhou, Weidong Xie, Enrique J. Lavernia, Influence of extrusion on the microstructure and mechanical behavior of Mg-9Li-3Al-xSr alloys, Metall. Mater. Trans. A, Vol. 44, pp. 1103-1113, February, 2013.

13) Baolong Zheng, Ying Li, Weizong Xu, Yizhang Zhou, Suveen N. Mathaudhu, Yuntian Zhu and Enrique J. Lavernia, "Twinning in cryomilled nanocrystalline Mg powder", *Philisophical Magazine,* Vol. 93, pp. 457-464, June, 2013.

14) Baolong Zheng, Dalong Zhang, Yizhang Zhou, Suveen N. Mathaudhu, Deepak Kapoor, Joseph Paras, and Enrique J. Lavernia, Dynamic Grain Refinement in Nanostructured Mg and Mg-Y Deformed at Cryogenic Temperatures, PowderMet 2013, Chicago, IL, June 24-27, 2013;

15) Baolong Zheng, Yizhang Zhou, Suveen N. Mathaudhu, and Enrique J. Lavernia, Dynamic grain refinement for nanostructured pure Mg powder processed via cryogenic temperature deformation of cryomilling, the 2013 TMS Annual Meeting & Exhibition, March 3–7 San Antonio, Texas.

16) Yan Yang, Xiaodong Peng, Baolong Zheng, Yizhang Zhou, Enrique J. Lavernia, Microstructure and Mechanical Properties of Nanocrystalline Mg-9Li-3Al-2.5Sr Alloy via Cryomilling and Spark Plasma Sintering, the 2013 TMS Annual Meeting & Exhibition, March 3–7 San Antonio, Texas.

17) Dalong Zhang, Baolong Zheng, Yizhang Zhou, Suveen Mathaudhu, Enrique Lavernia, "Deformation Behavior of Nanocrystalline Mg-Y Alloy", the 2013 TMS Annual Meeting & Exhibition, March 3–7 San Antonio, Texas.

18) Dalong Zhang, Baolong Zheng, Yizhang Zhou, Subhash Mahajan and Enrique J. Lavernia, Prism stacking faults observed contiguous to a {10-12} twin in a Mg–Y alloy. Scripta Materialia, Vol. 76, pp. 61-64, 2014.

19) A Williamson, B Zheng, E Lavernia, J Groza, J-P Delplanque, Investigation of Pressure and Thermal Behavior during Spark Plasma Sintering on Grain Growth, TMS2014, San Diego, CA. February 16-20, 2014.

20) Baolong Zheng, Yizhang Zhou, Suveen N. Mathaudhu, Ruslan Z. Valiev, Chi Y.A. Tsao, Julie, M. Schoenung, and Enrique J. Lavernia, Multiple and Extended Shear Band Formation in MgCuGd Metallic Glass during High Pressure Torsion, Scripta Materiala, 2014 (Accepted).

2. Scientific Personnel

Dalong Zhang, Graduate Student
Yan Yang, Visiting Graduate Student
Dr. Osman Ertorer, Post-doctoral Researcher
Dr. Ying Li, Post-doctoral Researcher
Dr. Baolong Zheng, Assistant Project Scientist
Dr. Yizhang Zhou, Associate Researcher

3. Scientific Progress and Accomplishments

This report covers the research activities completed during the period from October 1, 2010 to December 31, 2013. Key research activities conducted in this reporting period include: (1) synthesis of nanostructured pure Mg and Mg alloy powders by cryomilling; (2) analysis of deformation twinning in nanostructured Mg and Mg alloy powders; (3) synthesis, microstructural and mechanical characterization of bulk nanostructured pure Mg and Mg alloys; (4) synthesis of nanostructured Mg-Y powders by gas atomization and cryomilling; (5) investigation of stacking faults and twinning in a high strength, ductile ultrafine grained Mg-Y alloy; (6) mechanical characterization of ultrafine grained Mg-Y alloy; (7) dynamic grain refinement in nanostructured Mg and Mg-Y deformed at cryogenic temperatures; (8) influence of mechanically milled powder and high pressure on spark plasma sintering of Mg-Cu-Gd metallic glasses; (9) microstructure and mechanical behavior of Mg-10Li-3Al-2.5Sr alloy; (10) influence of extrusion on the microstructure and mechanical behavior of Mg-9Li-3Al-xSr alloys; (11) study of multiple and extended shear band formation in MgCuGd metallic glass during high pressure torsion; and (12) observation of prism stacking faults contiguous to a {10-12} twin in a Mg–Y alloy. The key findings generated from the aforementioned research activities #1-10 have been reported in the previous three annual progress reports (e.g., 10/2010-07/2011, 08/2011-07/2012 and 08/2012-07/2013). Accordingly only key accomplishments associated with #11-12 efforts are described in detail in the present report.

3.1. Multiple and Extended Shear Band Formation in MgCuGd Metallic Glass during High Pressure Torsion

$Mg_{65}Cu_{25}Gd_{10}$ bulk metallic glass (BMG), containing a high density of intersecting extended shear bands (SBs), was fabricated from densification of amorphous powder via high pressure torsion (HPT). The extended SBs, up to 400 nm in width and containing nanocrystalline (nc) structures, were studied using SEM and TEM. The mechanisms responsible for the formation of the high density extended SBs are discussed and related to the high hydrostatic pressure and shear strains imposed during HPT of the BMGs.

High-pressure torsion (HPT), one of severe plastic deformation (SPD) techniques, introduces large amounts of plastic deformation via rotation of a disk-shaped specimen under high pressures (typically higher than 4 GPa). The characteristics of HPT processing include high hydrostatic pressure and large superimposed shear strains (γ >1000, equivalent to true strain ε of 6.9, can be achieved) with a limited temperature increase (e.g., <283 K).

Inspection of the literature reveals few studies describing HPT processing of BMGs, partly due to the poor formability and plasticity of BMGs at room temperature. Different from crystalline metals, deformation via dislocation and twinning mechanisms is not possible in the case of BMGs. BMGs deform in a highly localized mode, where a large amount of plastic strain is accumulated in very thin (~10 nm – 100 nm) narrow regions, known as shear bands (SBs), which are important in BMGs because the associated strain-softening leads to plastic instability during deformation. It has also been reported that the formation of multiple SBs throughout a BMG sample can enhance its plasticity via the introduction of "plastically soft" regions. Because each band contributes to the overall plasticity and none carry sufficient deformation to cause catastrophic failure, room temperature formability can be enhanced.

In this research we report, for the first time, the synthesis of BMGs by consolidation of amorphous powder using HPT, paying particular attention to mechanisms governing the in-situ formation of a high density of extended SBs with nanocrystalline (nc) grains. The objective of our study is to provide preliminary insight into the mechanisms that govern the initiation, activation and behavior of SBs formed during HPT, using SEM, TEM, and DSC results as the basis.

In our experiments, gas atomized $Mg_{65}Cu_{25}Gd_{10}$ amorphous powder, with an approximate size of 150 μm, was processed via HPT under a pressure of 6 GPa and five turns at room temperature. The turning speed used in these experiments was 0.2 rpm. BMG disks approximately 10 mm in diameter and 1 mm in thickness were prepared using this procedure.

TEM studies were conducted on thin foils of the HPT processed MgCuGd BMGs and were prepared via mechanical grinding and polishing to a thickness of about 30 μm, followed by ion milling (Gatan PIPS-691) to a thickness suitable for electron transparency. A Philips CM-12 transmission electron microscopy (TEM) was used for TEM micrograph and selected area electron diffraction (SAED) analysis.

Figure 3.1.1 shows the SEM micrograph of the MgCuGd BMG disk, which was consolidated via HPT of gas atomized amorphous powder. The SEM images were taken from positions near the upper surface (in contact with the rotating plunger) and near the center of the radius of HPTed BMG. The absence of cracks and interfaces between particles was evident on the surface of HPTed BMG disks. Generally, it is difficult to achieve complete inter-particle metallurgical bonding between the metallic glass powders due to the presence of a surface oxide film, which acts as a diffusion barrier and limits the mass transfer. In the case of HPT, however, the action of intense shear strains (about 150, equivalent to true strain ε of 5, for our samples) and normal compressive stresses (6 GPa) effectively disrupt surface oxides, thereby enhancing kinetics of interface metallurgical bonding formation between particles.

Figure 3.1.1(a) shows that there is a high density of SBs on the surface of HPTed MgCuGd BMGs. Moreover, multiple-SBs can be discerned as vein patterns with different orientations. It was also observed that there are some primary SBs, with a thickness >100 nm, and a large amount of secondary SBs with a thickness <100 nm, as highlighted by arrows in Figures 1(a) and (b). The secondary SBs appeared to have originated at primary SBs, and evolved with different orientations. The patterns of primary and secondary SBs exhibit spacing of 1–2 μm and 0.2–0.6 μm, respectively. The presence of a high density of SBs can be rationalized on the basis of the imposition of high shear strains in combination with a high hydrostatic compression stress during HPT processing, which can suppress SB separation, and thereby avoid premature crack nucleation as in the case of tension. Hence the presence of a high hydrostatic compression stress during HPT effectively promotes the formation of multiple SBs, which can better accommodate deformation.

The origin of the observed network of SBs can be explained on the basis of the interactions between the SBs, which increase the local stress field and nucleate SB branches to release localized stress concentration and accommodate surrounding shear strains. During HPT, SBs that are initiated in high stress or plastically soft regions are arrested in surrounding regions having a higher yield stress or stiffness, or at an intersecting SBs. This inhomogeneous mode of deformation occurs under conditions of high applied stresses and temperatures lower than T_g. In the presence of a high hydrostatic compression stress, the primary SBs can grow continuously and carry the plastic strain without nucleating cracks. Moreover, some small, wing-like branch bands were found along primary SBs, suggesting that the SB branches can grow and interact leading to the formation of a network that can sustain the overall strain during deformation. The primary SBs appear wavy, and the periodicity of the wave is about 0.2 to 0.6 μm, which is consistent with the observed interspace between secondary SBs. It was reported that the room temperature formability of BMGs can be enhanced by introducing "plastically soft" regions. Hence, even though the plastic strain is localized in the SBs, the BMGs appear to deform in a macroscopically near-homogenous manner due to the formation and presence of a network of SBs. In fact, during initial loading, the formation of SBs will contribute to the overall plastic deformation of the powders, whereas after full densification is achieved, the network of SBs (as soft regions) enhances the overall plasticity of the BMG.

Deformation during HPT is highly localized in the SBs, leaving most of the sample un-deformed. The TEM images of the HPTed MgCuGd BMG, shown in Figure 3.1.2, were taken from positions corresponding to the center of the HPTed BMG, both in thickness and radial directions. The corresponding histograms for the thickness of SBs and grain size distributions of crystals in SBs are also shown in Figure 3.1.2 (a) and (b), respectively. The TEM bright field images reveal the presence of a featureless amorphous phase. Neither precipitates nor any type of phase contrast was evident in these amorphous regions of the sample. In addition to revealing the presence of a high density of SBs in the TEM images of the HPT processed MgCuGd BMGs, the extended SBs were measured to have thickness values that ranged from 50 nm to 400 nm, and an average of 214 nm; this is in contrast to published work which reports shear-band thickness values of 10–20 nm.

The physical characteristics of the SBs provide insight into the deformation of the MgCuGd BMG during HPT. In related work, it was reported that the formation of SBs results local planar heating, which can cause local heating above T_g, crystallization as shown in Figure 3.1.2. The temperature profile, ΔT, as a function of t and of distance x from the SBs can be determined from:

$$\Delta T = \left(\frac{H}{2\rho C\sqrt{\pi\alpha}}\right)\frac{1}{\sqrt{t}}\exp\left(\frac{-x^2}{4\alpha t}\right) \quad (1)$$

where H is the heat content, ρ is the density of the material, C the specific heat and α the thermal diffusivity. The local heating at a SB results in a normal distribution in the temperature profile along the cross-section of a SB. The temperature rise at the center of SBs, T_{center}, when shear stops (at t =0) can be expressed by:

$$\Delta T_{center} = \frac{1}{\sqrt{\pi}}\left(\frac{H}{\rho C}\right)\sqrt{\frac{1}{\alpha\delta t}} = \frac{1}{\sqrt{\pi}}\left(\frac{H}{\rho C}\right)\sqrt{\frac{V}{\alpha y}} \quad (2)$$

where δt is the duration of shear at relative velocity V giving a shear offset $y=V\delta t$. The corresponding estimate of T_{center} is over thousand K, and the thermal diffusion length 2(αt)1/2, doubled to give a total width 100–300 nm. When high local heating reaches T_g or T_x, viscosity inside the SBs suddenly decreases, resulting in superplastic deformation of the metallic glass localized into SBs. In conventional uniaxial tensile and compressive deformation, the initiation and propagation of SBs is generally instantaneous leading to catastrophic brittle failure of BMGs; hence there is not sufficient time for the SB's thickness to increase. In contrast, the presence of a high hydrostatic pressure during HPT effectively suppresses crack nucleation and continuous shear deformation in the SBs causes local heating, which promotes thickening of the SBs and localized crystallization of nc grains (<100 nm) in the extended SBs.

It is worth noting that close inspection of the extended SBs reveal the presence of nc grains with an approximate size of 62 nm, as shown in Figure 3.1.2(b). The nc grains are responsible for the rings in the selected area electron diffraction (SAED) pattern shown in the inset figure. The presence of these nc grains within the SBs can be attributed to local planar heating generated during highly localized shear deformation. Moreover, it was also observed that there were some sub-SBs in the vicinity of the interface formed between the crystallites and the amorphous matrix in the primary extended SBs. Figure 3.1.2(c) shows a high magnification view of four sub-SBs located inside one SB, approximately 400 nm thick. The thickness of sub-SBs ranges from 15 nm to 45 nm, and increases as one moves from the center to the edge of the SBs. Extended exposure to high localized heating in the vicinity of SBs during HPT results in crystallization of a high density of nc grains in the primary SBs. Consequently, shear deformation remains localized in these extended and crystallized SBs, and promotes the formation of sub-SBs as illustrated in Figure 3.1.2(c).

The observed increase in density and thickness of SBs as a function of radial distance from the center of the HPT sample is consistent with the associated increase in strain towards the edge of the disk. The nominal effective shear strain can be estimated on the basis of the following equation: $\gamma=2\pi RN/t$, equivalent to true accumulated strain $\varepsilon=ln(2\pi RN/t)$, where N is the number of rotations, R is the distance from the center of the rotation, and t is the thickness. The deformation shear strain increases from the center to the edge of an HPT processed BMG disk; decreases with increasing sample thickness; and increases with increasing number of HPT turns. It then follows that the density and thickness of SBs increase with increasing number of HPT turns.

Figure 3.1.3(a) shows DSC trace patterns corresponding to as-atomized MgCuGd powders and HPT processed BMGs, as determined using a heating rate of 20 K/min. The glass transition temperatures, T_g, reveal only a negligible increase, whereas the crystallization onset temperature, T_x decreases significantly after HPT processing. T_x decreases from 479 K to 460 K for the HPT processed MgCuGd BMG. It is likely that structural relaxation occurred in the HPT processed BMGs as T_x decreased, which is a result of the strain energy introduced during HPT processing before crystallization eventually occurs. The physical mechanism of structural relaxation in BMGs involves stress relief, atomic movement and the annihilation of excess free volume. Both high pressure and shear deformation during HPT can promote short-range atomic rearrangement in BMGs by reducing the free volume. We propose that in our experiments, SB formation was assisted by the extreme localization of shear in terms of a structural change, a temperature rise, and a local viscosity decrease in the bands. It is known that there are three stages for initial SB formation: the multiplication of free volume; the coalescence of free volume and formation of voids; and the final fast propagation of SBs/cracks. Therefore, the formation of SBs is also closely related to local structural relaxation, which is consistent with our results. For HPTed BMG disc, it is also interesting to note that there is two-step crystallization, which may be rationalized as precipitation of other intermetallic compounds from the amorphous phase in addition to structural relaxation, and requires additional work.

Because of the sample size and geometry, only micro-indentation deformation studies with different applied loads, 50 g to 1000 g, were carried out. Results show that indentation size increases linearly with applied load. An average Vickers micro-hardness value of approximately 306 HV was obtained from measurements across the HPTed MgCuGd disk, which corresponds to an approximate strength of 1000 MPa from micro-hardness

values. It is interesting to note that no cracks were evident in the samples, even for large indents obtained with a 1000 g load force, as shown in Figure 3.1.3(b). This apparent ductility may be rationalized based on the presence of existing multiple SBs, which contribute to shear softening, and therefore, plasticity during indentation. It is well known that crystalline metallic materials can exhibit high macroscopic plastic deformation due to multiple cross slip. Similarly, our results suggest that it is possible to introduce large amounts of plasticity into BMGs by generating a high density of multiple and interacting SBs under a high superimposed hydrostatic stress, as shown in Figures 3.1.1 and 3.1.2.

Figure 3.1.4 provides a schematic diagram illustrating the influence of shear deformation during HPT on the resultant stress-strain response, and can be described as follows. In the case of a primarily tensile stress state, SBs nucleate and rapidly evolve into cracks without much growth, resulting in catastrophic brittle failure before yielding (a). In the case of a uniaxial compressive stress state (b), thin SBs nucleate in the BMG matrix, and continue to deform to slightly beyond yielding due to compressive stress confining the shear band. Finally, in the case of a high superimposed hydrostatic compressive stress (c), such as HPT, multiple extended SBs nucleate in the BMG matrix and continue to deform and interact during deformation, possibly even leading to strain-softening.

In summary, Mg-based MgCuGd BMGs were successfully fabricated via HPT consolidation directly from gas atomized powders. A high density of extended SBs containing nc grains developed during HPT of MgCuGd BMG, and this phenomenon was attributed to the combination of intense shear deformation under an imposed hydrostatic pressure.

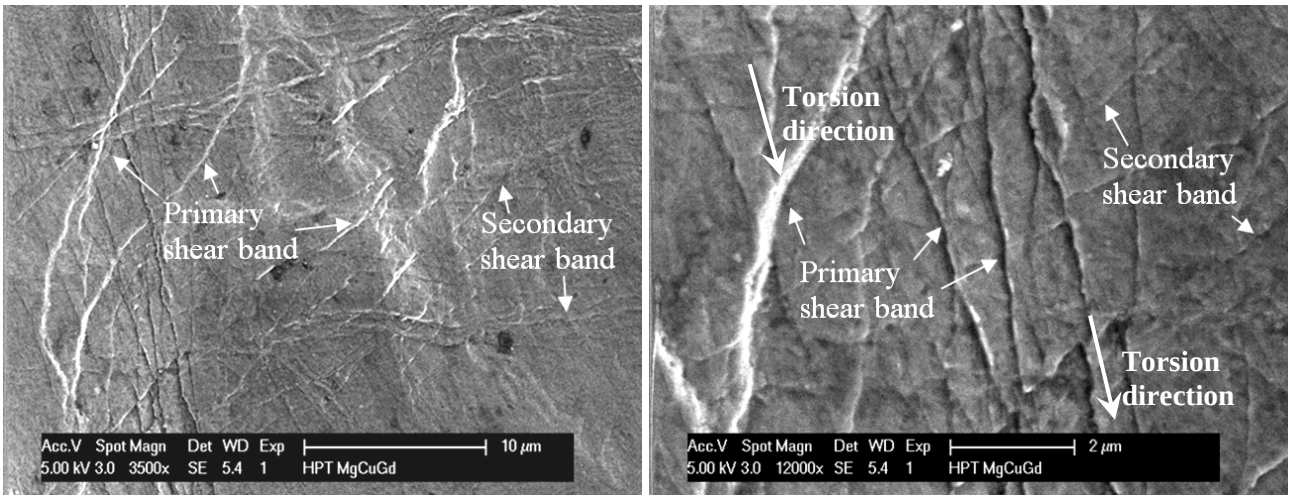

(a) (b)

Figure 3.1.1. High density of SBs in HPT processed MgCuGd BMG (a) low magnification SEM image, and (b) magnified SEM image.

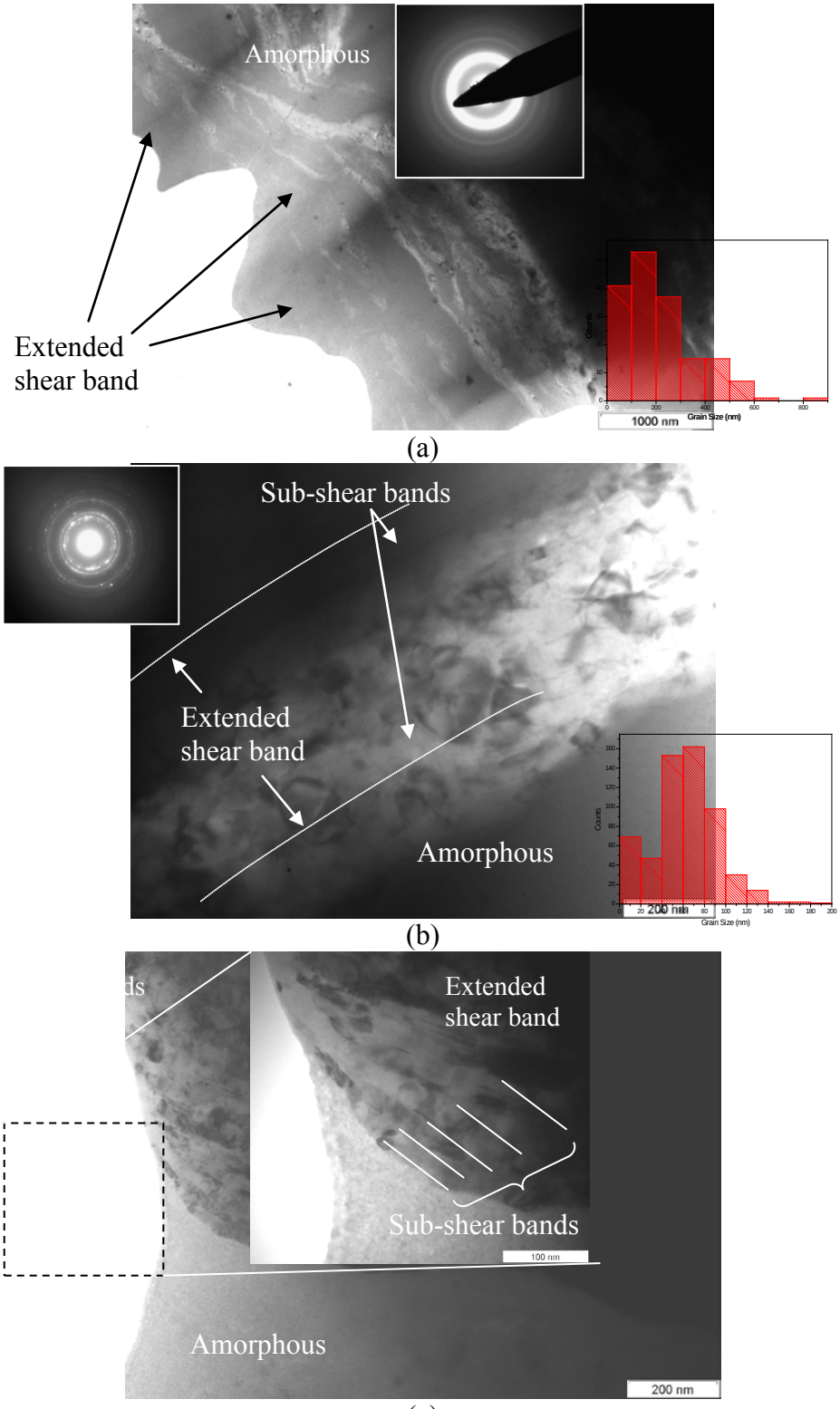

Figure 3.1.2. Extended SBs in in HPT processed MgCuGd BMG: (a) low magnification TEM image with SAED pattern and histograms for SB thickness, (b) magnified TEM image of local SB with SAED pattern and histograms for grain size of crystals, and (c) sub-SBs inside extended SBs.

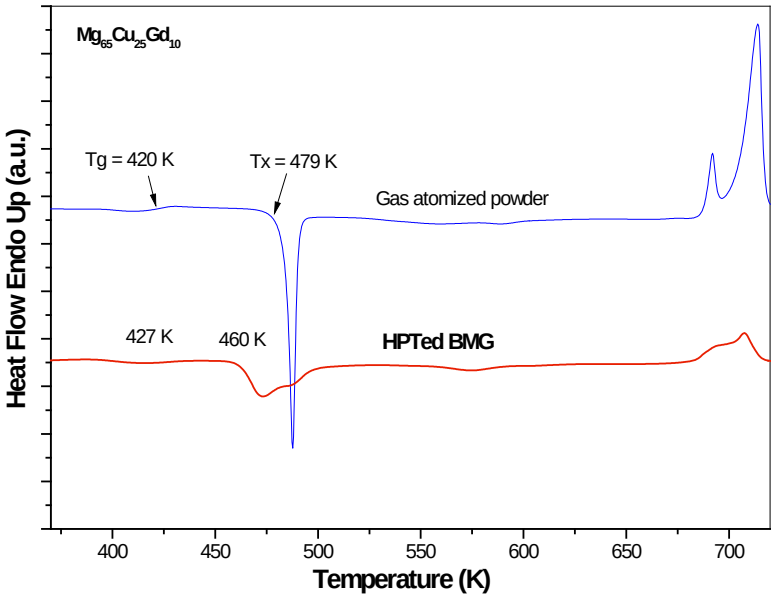

(a)

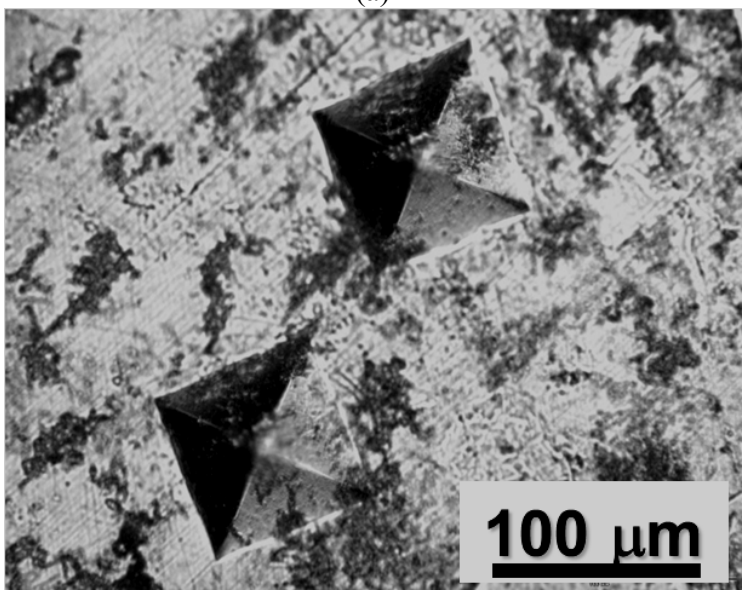

(b)

Figure 3.1.3. (a) DSC patterns of HPT processed bulk MgCuGd BMG compared with starting MgCuGd powder, and (b) Vickers microhardness indentation with 1000 g load force.

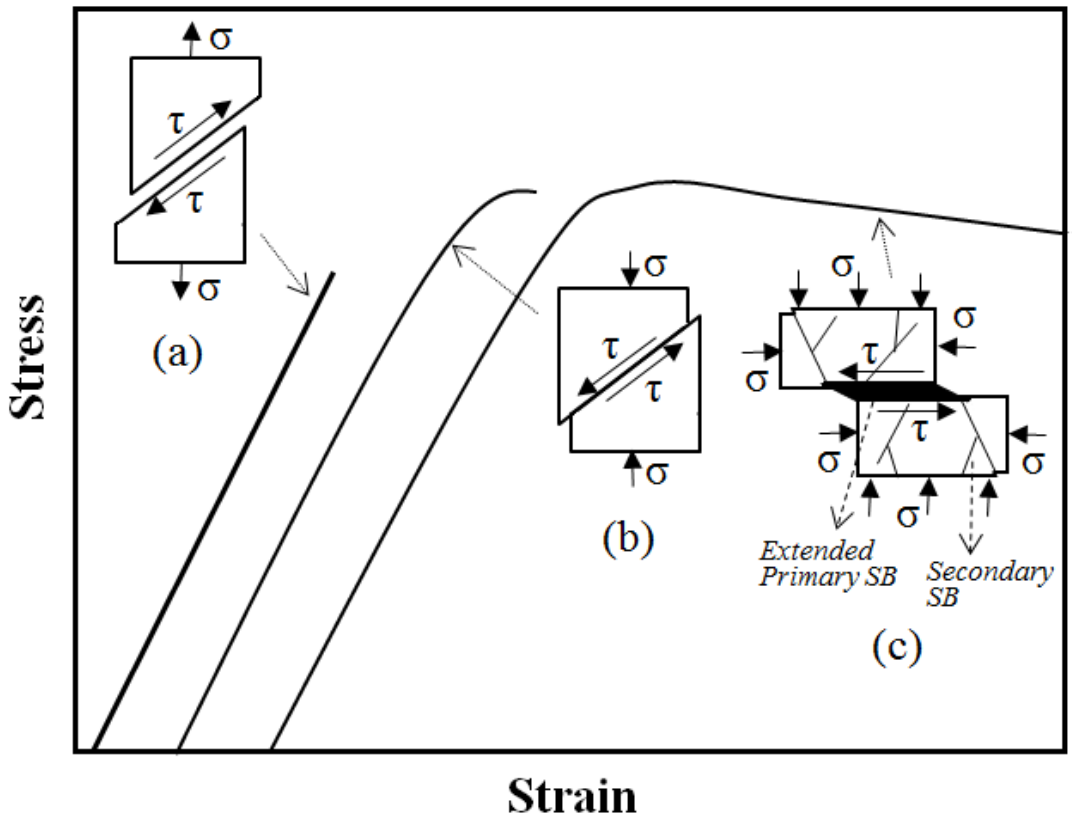

Figure 3.1.4. Illustration of SB evolution in BMGs as a function of shear strain and stress states with (a) tensile stress, (b) uniaxial compressive stress, and (c) hydrostatic compressive stress, such as HPT.

3.2 Prism stacking faults observed contiguous to a {10-12} twin in a Mg–Y alloy

In view of the lack of fundamental understanding on the interactions between SFs and twins, and prism dislocation activity in Mg–Y alloys, we studied an Mg–Y alloy to provide experimental insight into non-basal deformation modes, e.g. twinning and prism slip/stacking faults, and their possible interactions. Mg–2.5 at.% Y alloy powder was synthesized by melting Mg–30 wt.% Y master alloy with pure Mg at 800 °C, followed by gas atomization in an Ar atmosphere. After hot vacuum degassing, the powder was consolidated via hot isostatic pressing and extrusion (reduction ratio 10:1) at 350 °C, resulting in a fine-grained (FG) Mg–Y alloy (grain size 1–2 μm). Cylindrical specimens, 5 mm in diameter and 7 mm in height, were machined and polished for compression along the extrusion direction (ED) at a strain rate of 10^{-3} s^{-1} and at room temperature. The FG Mg–Y exhibited a yield stress of ~310 MPa, an ultimate compression stress of ~430 MPa and a strain to failure of ~22%. In this study, we specifically focus on a specimen that was deformed to ~2% strain along the ED. Thin foils for transmission electron microscopy (TEM) studies (JEOL JEM 2500 SE, 200 kV) were ground to a thickness of ~30 μm, followed by ion milling until perforation.

It is well known that, when compressed along the ED, {10-12} deformation twins form readily in Mg alloys [10-11]. Figure 3.2.1 shows part of a microsized grain in a sample compressed to ~2% strain along ED. The grain was observed in the <1-21-3> zone axis (Fig. 3.2.1b). There is an obvious band-like region with white contrast (Fig. 3.2.1a), indicating the presence of {10-12} deformation twins. There is also a high density of line contrast within the twin (region B in Fig. 3.2.1a), suggesting the presence of basal plane SFs.

To study the twin boundaries (TBs) and SFs in more detail, dark-field (DF) images (Fig. 3.2.1d and f) were obtained using the 10-10 diffraction spot in Figure 3.2.1b. In this format, the parent grain will appear bright whereas the {10-12} twin will appear dark. Comparing the DF images (d and f in Fig. 3.2.1) with the corresponding bright-field (BF) images (c and e in Fig. 3.2.1), one can clearly see the nearly straight TBs

(marked as dashed yellow lines). Interestingly, SFs not only lie in the twin, but also extend into the parent grain (e.g. SFs highlighted by yellow and red arrows in Fig. 3.2.1e) – although, for the parent grain, the (0001) basal plane cannot be viewed from the <1-21-3> zone axis. Instead, the orientation of the SFs in the parent grain aligns with that of (10-10) prism planes, as evidenced by the diffraction pattern in Figure 3.2.1b. Accordingly, one may conclude two observations: first, there are indeed SFs located inside the parent grain, and second these are prism SFs.

It is important to note, however, that the dashed yellow lines which highlight the TBs in the BF–DF TEM analysis represent an approximate location of TBs for the following reasons. First, since the twinned region is not close to any zone axis, it is very difficult to observe the TBs precisely edge-on in TEM. Second, a twin is a three-dimensional structure, so it is possible for the twin to be inclined to the viewing plane (e.g. (1-21-3)), and thereby overlap with the parent grain in the projected TEM view. Third, real TBs can deviate significantly from the ideal {10-12} twin plane in deformed hcp materials, which is probably due to the steps created by twin–slip interaction.

Therefore, to provide additional experimental evidence to the suggestion that there are SFs on the (10-10) prism planes in the parent grain, as opposed to the possibility that these are overlapping basal SFs in the {10-12} twin with the parent grain, we employed high-resolution TEM (HRTEM) and fast Fourier transformation (FFT). In reciprocal space, an SF will resemble a slender rod in appearance. Figure 3.2.2 shows the HRTEM image of some SFs in the parent grain (e.g. region A in Fig. 3.2.1e). Figure 3.2.2b and d are FFT images for selected areas (red squared areas I and III in Fig. 3.2.2a) containing no SFs, and they are the same pattern as the diffraction pattern in Figure 3.2.1b, i.e. these areas are indeed at the h1-213i zone axis. For the selected area (SA) II, which contains the tip of one SF, the FFT shows streaking (highlighted by red arrows in Fig. 3.2.2c) that connects spots for the (-1010) and (10-10) planes. These observations support the suggestion that the SFs in Figure 3.2.2a are indeed prism SFs. Furthermore, Figure 3.2.2e is the inverse FFT image for SA II in Figure 3.2.2a, and it was obtained by selecting the -1010 and 10-10 pair spots; therefore it shows the (10-10) atomic planes. It is noted that there is no extra half (10-10) plane in Figure 3.2.2e, which indicates that the prism SFs are the results of Shockley partial activity in (10-10) planes.

At low magnification, the contrast for SFs in the twin and parent grain appears to be similar; namely, when crossing the TB, the change in contrast for two types of SFs is barely perceptible. However, when observed at high resolution at the same <1-21-3> zone axis for the parent grain, as evident in Figure 3.2.3a, the contrast for basal planes and basal SFs in the {10-12} twin (e.g. region B in Fig. 3.2.1e) is diffuse and unclear, unlike the contrast for prism planes and SFs in the parent grain (e.g. Fig. 3.2.2a). Figure 3.2.3b shows the FFT for a selected area in Figure 3.2.3a (red square) containing basal SFs, and the blue arrows indicate the streaking caused by basal SFs. This suggests that, in the {10-12} twin, the basal planes and SFs are near edge-on, whereas other planes are not.

Experimental observations of prism SFs in other hcp materials, e.g. Ti and Zr, were first reported several decades ago. However, this is the first direct TEM observation of prism SFs in hcp Mg alloys. It is also worth noting that prism SFs were only observed in the vicinity of the {10-12} twin (e.g. area A and C in Fig. 3.2.1c); there is no such contrast anywhere away from the {10-12} twin. Therefore, to understand the underlying mechanism(s) responsible for the formation of these prism SFs, the relationship between prism SFs in the parent grain and basal SFs in {10-12} twin was investigated, as discussed below.

Niewczas [1] calculated the mathematical transformation matrices required to link the parent lattice with twinned lattice for hcp crystals. This makes it possible to quantitatively calculate the misorientation between a plane in the parent grain and a plane in a twinned lattice. For example, for a (-1012) [10-11] twin, the misorientation between the (10-10) prism planes in the parent grain ((10-10)P) and the (000 1) basal planes in the twin ((0 001)T) was calculated to be ~2°. This calculated value is consistent with our observation that, when the prism SFs/(10-10)P in the parent grain are located edge-on at <1-21-3> zone axis (Fig. 3.2.2c), the contrast

of basal SFs/(0001)T in the twin can also be seen (e.g. region B in Fig. 3.2.1c). This confirms the suggestion that the twin studied here is indeed a {10-12} twin – specifically, a (-1012) [10,11] twin variant.

Niewczas [1] also summarized the possible relationship between slip systems in a {10-12} twin and that in the parent grain from a geometrical standpoint. It is noted that (10-10)[-12-10] prism slip in the parent grain can be "transformed" to (0001) [1-210] basal slip in a (-1012) [10-11] twin. It then follows that (0001) [1-210] basal slip in a {10-12} twin could probably be transformed to (10-10)[-12-10] prism slip in the parent grain as well. Serra and Bacon [2] used computational simulations to predict the possible interaction of 1/3 <1-210> screw dislocation with TBs in hcp materials. They concluded that, in hcp Mg, it is possible for a 1/3 <1-210> screw dislocation in basal plane to propagate across a {10-12} TB and remain in the prism plane near the TB. In our study, careful examination of the configuration of SFs in the vicinity of the {10-12} twin reveals that there are multiple types of SFs: prism SFs (e.g. those highlighted by red arrows in Fig. 3.2.1e), basal SFs (e.g. highlighted by blue arrows in Fig. 3.2.1c) and "compound SFs" – namely, SFs with one end in the parent grain and the other end in the twin (e.g. SFs highlighted by yellow arrows in Fig. 3.2.1e). In addition, in Figure 3.2.1e there are also SFs spanning from the left part of the parent grain across the entire twin to the right part of the parent grain. These results probably suggest very dynamic partial dislocation activity across the TBs.

On the basis of the above discussion, together with the fact that there is no extra half atom plane in Figure 3.2.2e, it is proposed that the prism SFs observed here are the results of dissociated 1/3 h1-210i dislocations transmitted from (0001)T to (10-10)P. Figure 3.2.4 provides schematic illustrations of the proposed partial dislocation mechanisms. First, due to the reduced basal stacking fault energy by the alloying element Y and the twinning deformation, there are basal SFs in {10-12} twins bounded by 1/3 <1-100> Shockley partials, as shown in Figure 3.2.4a. Then, during incremental deformation, as shown in Figure 3.2.4b, some leading partials start to transmit through the TB to prism planes in the parent grain, while the trailing partials may also transmit (resulting in prism SFs) or remain in the twin (resulting in compound SFs). This transmission is geometrically possible because the three planes involved herein, namely (0001)T, (10-10)P and the twin plane (-1012), share the same intersection line [1-210]. Therefore, for example, a 1/3[1-100] partial dislocation in (0001)T can glide to TB, cross the [1-210] intersection line and get into (10-10)P; due to the change in indexation [1], this partial would assume a Burgers vector of 1/3[-1100]. It is noted that whether the leading and/or trailing partials transmit through TBs or not depends largely on the local stress concentration at the TBs, so different partials would behave differently – resulting in multiple configurations of SFs, as discussed above. However, the stress required for the partial dislocations to move further into prism planes is probably much higher than that in basal planes, since it is the case for 1/3 <1-210> full dislocations. This, we believe, is the reason why prism SFs were only observed in the vicinity of the {10-12} twin.

In this study, SFs can be considered as "markers" that can trace the activity of partial dislocations. However, it is also possible for full 1/3 <1-210> basal dislocations in a {10-12} twin to transmit to prism planes in the parent grain. This suggests that twinning in Mg and Mg alloys is a very dynamic and complex process, which involves interaction between (partial) dislocations, TBs and SFs. Particularly, the possible transmission of (partial) dislocations through TBs should be examined, for it could make deformation more compatible [1]. In addition, both basal SFs and prism SFs can serve as barriers for slip in other planes, resulting in strengthening. For example, prism SFs can impede the easy basal slip in Mg and Mg alloys. Therefore, the Mg and hcp materials research community probably needs to take a more comprehensive approach to better understand the underlying deformation mechanisms.

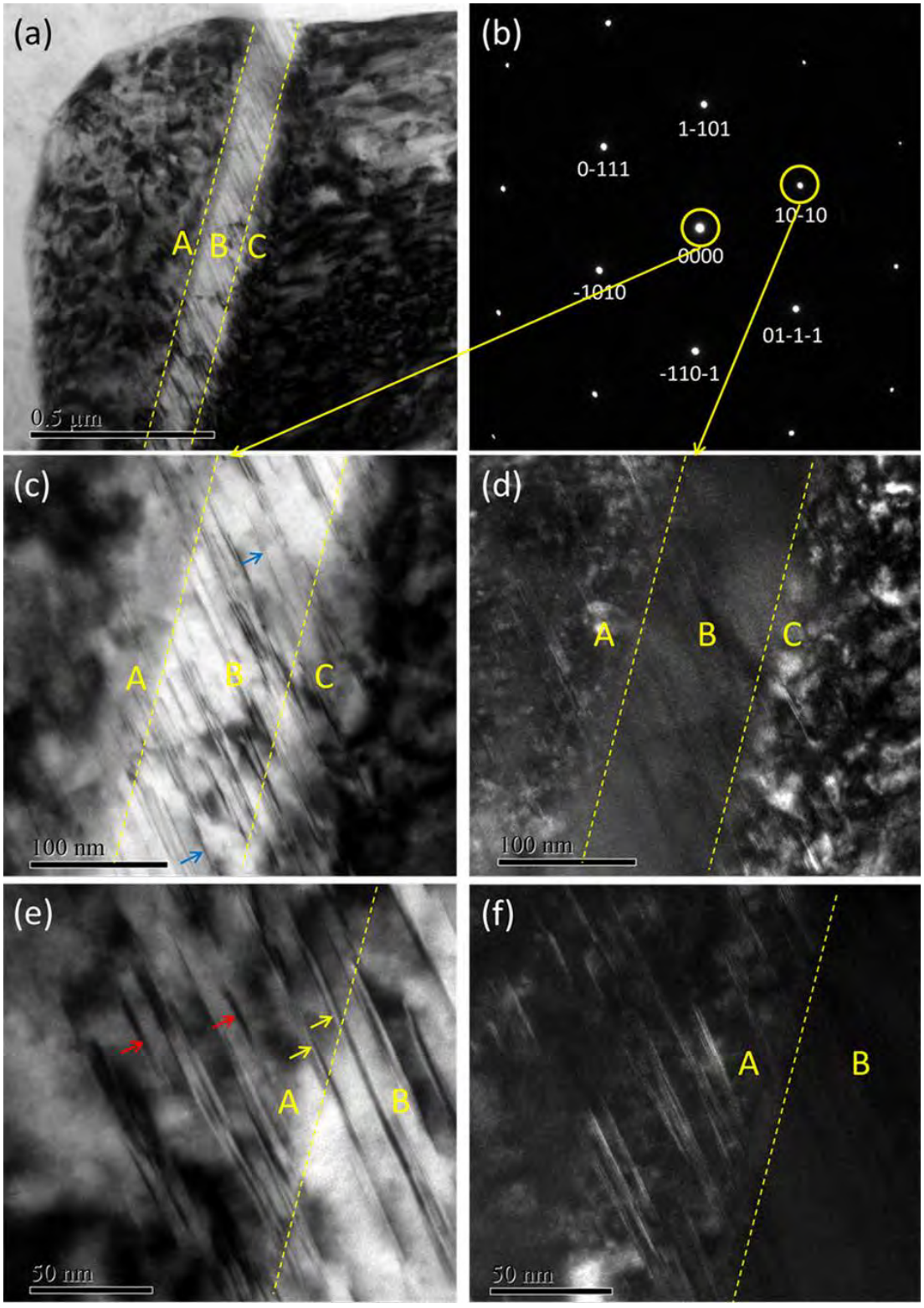

Figure 3.2.1. (a) Part of a microsized grain. (b) Selected area electron diffraction pattern of the parent grain. (c, e) Bright-field images for the {10-12} twin in (a). (d, f) Corresponding dark-field images for the same areas in (c) and (e), respectively.

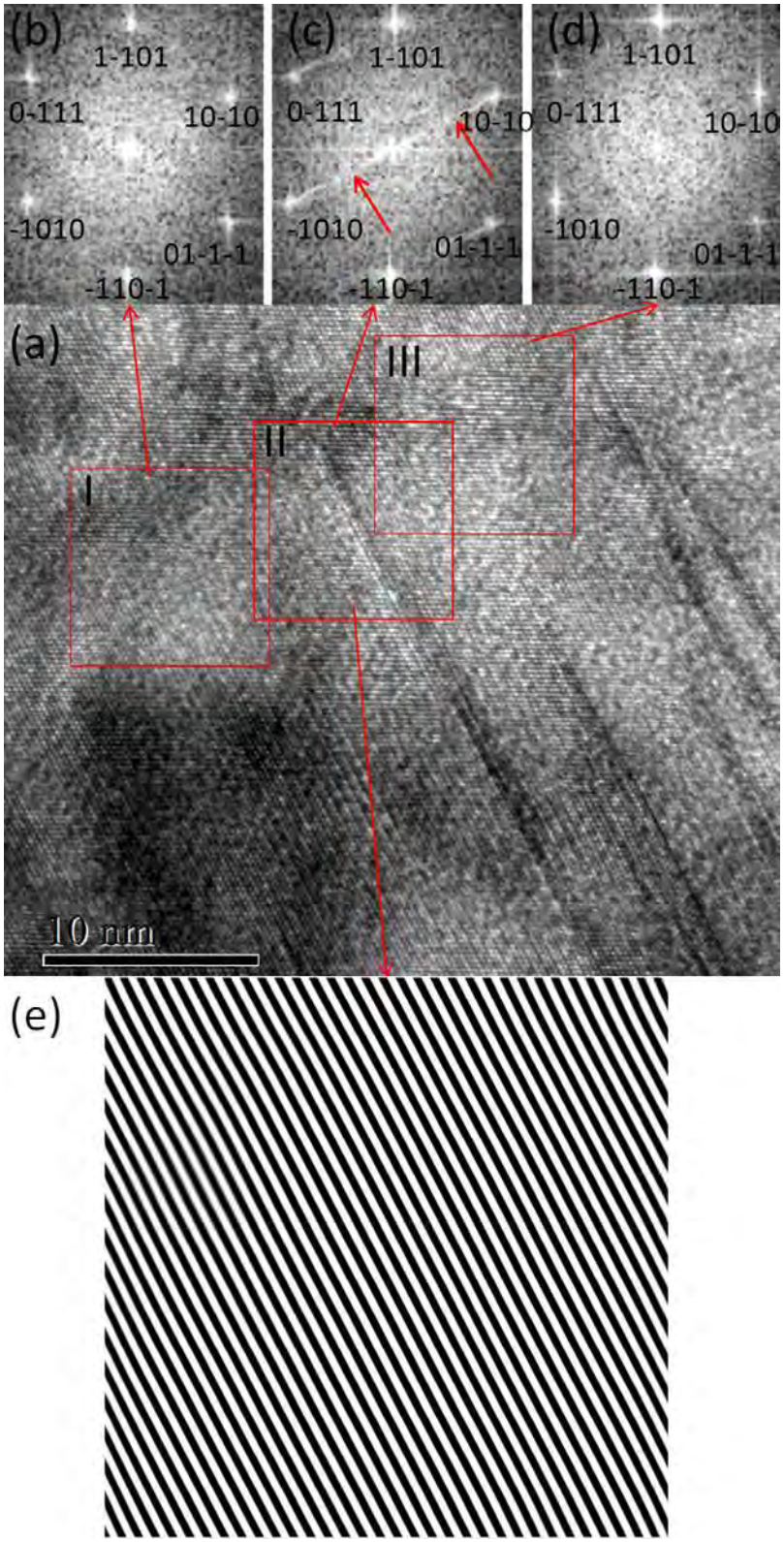

Figure 3.2.2. (a) HRTEM for prism stacking faults in the parent grain. (b–d) Selected area FFT around an SF. (e) Inverse FFT showing the {10-10} prism planes in area III.

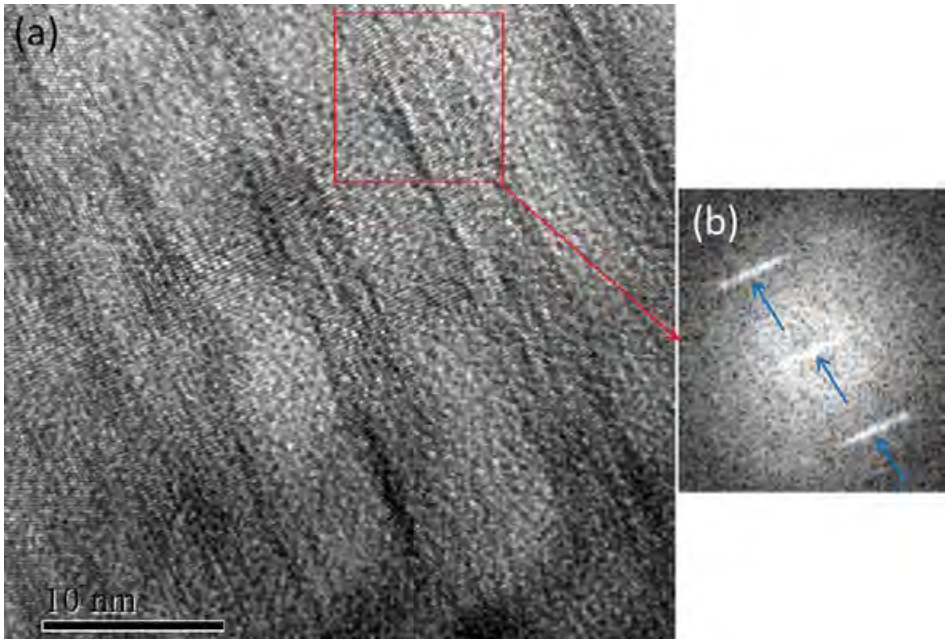

Figure 3.2.3. (a) Diffuse and unclear basal planes and SFs in a {10-12} twin. (b) FFT for a selected area in (a) (red square) containing basal SFs. (For interpretation of the references to colour in this figure legend, the reader is referred to the web version of this article.)

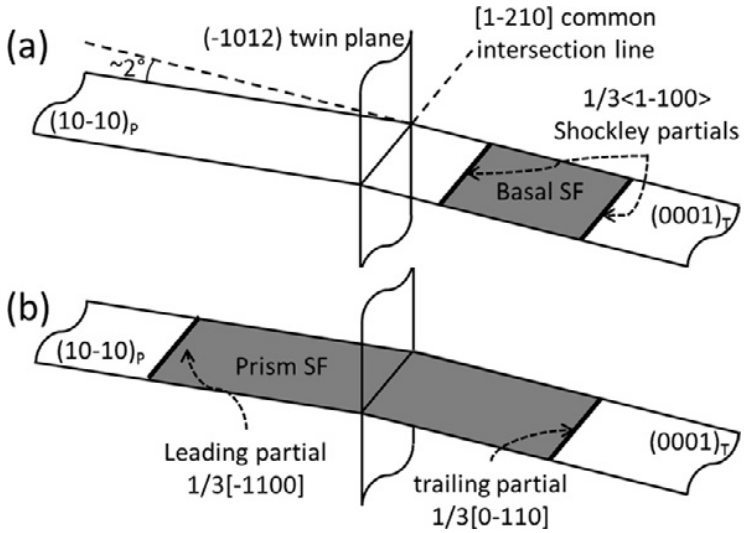

Figure 3.2.4. Schematics for formation of prism SFs.

References

[1] M. Niewczas, Acta Mater. 58 (2010) 5848–5857.
[2] A. Serra, D.J. Bacon, Acta Metallurgica et Materialia 43 (1995) 4465–4481.